Available online at website: https://journal.bcrec.id/index.php/bcrec

Bulletin of Chemical Reaction Engineering & Catalysis, 21 (2) 2026, 441-451

Original Research Article

Photocatalytic Activity of ZnO/Hydroxyapatite Nanocomposite for Remazol Red RB Removal in Aqueous Solution Under UV and Visible Light Irradiation

I Dewa Ketut Sastrawidana*, Luh Putu Ananda Saraswati, I Nyoman Sukarta, Ni Made Wiratini, I Ketut Sudiana, I Wayan Suja

Department of Chemistry, Faculty of Mathematics and Natural Sciences, Universitas Pendidikan Ganesha, Singaraja, 81116 Bali, Indonesia.

Received: 28th November 2025; Revised: 23th February 2026; Accepted: 24th February 2026
Available online: 10th March 2026; Published regularly: August 2026

Abstract

Textile industry wastewater contains synthetic dyes that are resistant to natural degradation, toxic, and capable of polluting aquatic environments. One commonly used dye is Remazol Red RB (RRRB), which is stable and difficult to remove through conventional treatment methods. Therefore, an effective approach is needed to break down this pollutant. This study aimed to develop and characterize a zinc oxide/hydroxyapatite (ZnO/HA) nanocomposite as a photocatalyst for degrading RRRB dye and to evaluate its photocatalytic performance under UV and visible light irradiation. The ZnO/HA nanocomposite was prepared by mixing ZnO and HA at a 1:1 ratio, followed by the addition of a small amount of water. The mixture was milled for 24 hours to obtain nanoscale particles. The resulting material was calcined at 700 °C and characterized using FTIR, XRD, and SEM-EDX to determine its physicochemical properties. Photocatalytic activity tests of the ZnO/HA nanocomposite toward RRRB dye solution were conducted in a batch system under 50-watt UV and visible light irradiation. The operational variables examined included catalyst dosage, initial pH, and dye concentration. FTIR analysis showed characteristic absorption bands of ZnO and HA, indicating successful formation of the nanocomposite. XRD results revealed a crystal size of 19.67 nm, while SEM-EDX confirmed the presence of Zn, Ca, P, and O elements, consistent with the nanocomposite composition. The degradation efficiency of 300 mL of 50 mg/L of RRRB solution at pH of 5 with 2.0 g of ZnO/HA nanocomposite under 50 watts of UV and visible light in succession was 90.43% and 80.93% for 120 minutes of irradiation.

Keywords: Photocatalytic degradation; Textile dye; UV and visible light; ZnO/HA nanocomposite

How to Cite: Sastrawidana, I. D. K., Saraswati, L. P. A., Sukarta, I. N., Wiratini, N. M., Sudiana, I. K., Suja, I. W. (2026). Photocatalytic Activity of ZnO/Hydroxyapatite Nanocomposite for Remazol Red RB Removal in Aqueous Solution Under UV and Visible Light Irradiation. *Bulletin of Chemical Reaction Engineering & Catalysis*, 21 (2), 441-451. (DOI: 10.9767/bcrec.20548)

Permalink/DOI: https://doi.org/10.9767/bcrec.20548

1. Introduction

Textile wastewater with high pollutant content, such as heavy metals, suspended particles, COD, dyes, and other persistent pollutants, is harmful to humans and the environment when it's discharged directly to the environment without prior treatment [1]. Approximately 10–50% of textile dyes are released into wastewater, and the textile industry is estimated to contribute about 17–20% of global water pollution [2]. The presence of colored effluents can reduce sunlight penetration, thereby hindering the photosynthetic activity of aquatic plants. Consequently, anaerobic microbial activity increases, leading to the production of foul-smelling by-products [3,4].

Several methods are currently employed to remove color from textile wastewater, including physicochemical processes like electrochemical oxidation, membrane separation, adsorption, photocatalytic degradation, advanced oxidation,

* Corresponding Author.
Email: ketut.sastrawidana@undiksha.ac.id
(I.D.K. Sastrawidana)

and coagulation [5-10]. Biological treatments using fungi and bacteria are also effective [11-13].

Semiconductor-assisted photocatalysis has become a popular and affordable green technology that uses photons to break down organic contaminants into innocuous byproducts. This method has drawn a lot of interest because of its non-selective oxidative characteristics and ability to mineralize organic contaminants into carbon dioxide and water [14]. In the photocatalytic degradation of pollutants, a semiconductor absorbs light energy at or above its band gap, resulting in electron-hole pairs. These photo-excited electrons and positive holes then participate in redox reactions that degrade pollutants [15]. The positive hole interacts with water molecules to produce highly reactive hydroxyl radicals (•OH), while photoexcited electrons react with oxygen molecules to generate superoxide radical anions ($\bullet O_2^-$). These reactive species (•OH and $\bullet O_2^-$) work to break down contaminants to harmless byproducts like CO_2 and H_2O [16,17]. The photocatalysis method has been widely used for the breakdown of various organic contaminants. It has also been applied in other domains, such as CO_2 reduction and disinfection [18].

Numerous semiconductors have been employed for photocatalysis, including tin oxide [19, 20], iron oxide [21], titanium dioxide [22], zinc oxide [23,24], and zinc stannate [25,26]. Among the available photocatalysts, $TiO_2$and ZnO are commonly used for treating pollutants in wastewater due to their non-toxicity, biocompatibility, and thermal and chemical stability [27-29]. However, the outstanding properties of ZnO, including lower toxicity profiles, stability, ease of synthesis, low material cost, and high biocompatibility, have encouraged the use of ZnO as a promising replacement for TiO_2 [30]. Although the band gap of ZnO is wider (3.37 eV) than TiO_2 in the anatase phase (3.20 eV), the electron mobility of ZnO is higher (200-300 $cm^2/V.s$) than TiO_2 (0.1-4.0 $cm^2/V.s$), leading to ZnO potentially better performance in photocatalytic applications [31,32]. However, ZnO faces several limitations, including its large band gap, which restricts its effectiveness to the UV spectrum, resulting in diminished visible light performance. Additionally, separating ZnO powder from the reaction solution and implementing continuous flow systems with ZnO presents significant challenges [33]. Several strategies have been undertaken to enhance the photocatalytic activity of ZnO and enable ZnO to operate under visible light, including doping with metals and non-metals and incorporating materials that function as catalyst supports [34]. The immobilization of ZnO onto a porous material's surface can effectively diminish the band gap energy. This transpires as a result of the establishment of a heterojunction between the ZnO and support materials, which can reduce the energy necessary for the generation of electron-hole pairs so that ZnO could be excited by visible light [35]. A number of porous materials, such as montmorillonite [36], graphene [37], and carbon [38, 39] have been utilized as potential photocatalyst support material composites for removing dyes from aqueous solutions.

Hydroxyapatite, a greener material with the chemical formula $Ca_{10}(PO_4)_6(OH)_2$, is an emerging catalytic support characterized by remarkable attributes, including large surface area, high mechanical and thermal strength, chemical stability, low water solubility, and large porosity [40,41]. In our previous work, hydroxyapatite synthesized using seashells via chemical precipitation was successfully employed as a support material for TiO_2 photocatalysts, enabling the degradation of RRRB dye in aqueous solutions [42]. The current work involves the preparation of ZnO/HA nanocomposites and the evaluation of their ability to degrade RRRB dye in wastewater using both UV and visible light irradiation. This study introduces a sustainable approach in the synthesis of new photocatalysts based on ZnO and HA sourced from seashells. This innovation provides an environmentally friendly and low-cost alternative as a calcium source for HA synthesis. The operational variables investigated include the effect of nanocomposite dosage, starting solution pH, and dye concentration on the efficiency of color removal.

2. Materials and Methods

2.1 Materials

Analytical-grade ZnO (99.9% purity; CAS No. 1314-13-2) was purchased from Sigma-Aldrich. The RRRB dye was sourced from a local textile dye supplier in Denpasar, Bali, Indonesia.

2.2 Preparation of ZnO/HA Nanocomposite

The ZnO/HA nanocomposite was prepared by blending HA and ZnO at a 1:1 weight ratio, followed by the addition of 60 mL of deionized water. The resulting suspension was milled for 24 hours using a bead milling machine to reduce the particle size to the nanoscale. Afterward, the product was dried at 105 °C for 5 hours and subsequently calcined at 700 °C for 3 hours to obtain the final nanocomposite.

2.3 Characterization of ZnO/HA Nanocomposite

FTIR (merk Shimadzu, type IRPrestige 21) analysis revealed the functional groups present in the ZnO/HA nanocomposite, SEM-EDX (merk FEI, type Inspect-S50) revealed its surface

morphology and elemental composition, and XRD (merk PANalytical, type X'Pert PRO) was employed to determine the crystal size.

2.4 Photocatalytic Degradation Performance

The photocatalytic degradation of RRRB dye was conducted in a batch reactor using ZnO/HA nanocomposites as the catalyst. A 300 mL aqueous solution of dye was placed in a reactor (25 × 12 × 10 cm^3), followed by the addition of the catalyst. The suspension was magnetically stirred at 150 rpm to ensure uniform dispersion. The reactor was immersed in a temperature-controlled water bath to maintain constant reaction conditions and irradiated with a UV lamp (YCRAYS, 395 nm, 50 W). The operational variables were investigated, including ZnO/HA nanocomposite dosage (1-2 g), initial pH (4-10), and dye concentration (25-75 mg/L). The solution pH was adjusted to the desired value by carefully adding hydrochloric acid (HCl) or sodium hydroxide (NaOH) solution dropwise under continuous stirring until the target pH was reached. Aliquots (5 mL) were collected at 15 min intervals over 120 min, filtered through Whatman No. 42 paper, and dye concentration was determined by measuring the absorbance at 518 nm using a UV–Vis spectrophotometer (Merk Shimadzu UV-2600i). With the same procedure, the photocatalytic degradation process is also carried out using visible light as a radiation source. The degradation efficiency of dye was calculated using the formula:

$$Degradation\ efficiency\ (\%) = \frac{Ao-At}{Ao} x\ 100\% \qquad (1)$$

Here, A_0 and A_t denote the dye's absorbance at the initial time and at time t, respectively.

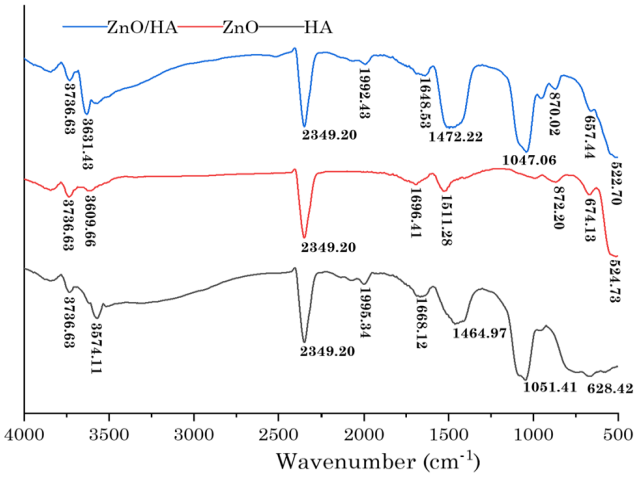

Figure 1. FTIR spectral profiles for HA, ZnO and ZnO/HA nanocomposite.

3. Results and Discussion

3.1. Characteristic of HA, ZnO, and ZnO/HA Nanocomposite

The functional group of the synthesized HA, ZnO, and ZnO/HA composite was observed using FTIR, and their spectra are presented in Figure 1. The FTIR spectrum exhibits several characteristic absorption bands that confirm the formation of hydroxyapatite. The prominent band observed at 3574.11 cm^{-1} corresponds to the stretching vibration of OH groups, while the band at 628.42 cm^{-1} is attributed to the librational mode of OH. The simultaneous presence of these two bands is widely recognized as a distinctive signature of crystalline hydroxyapatite. The strong absorption at 1051 cm^{-1} and 1995.34 cm^{-1} is assigned to the asymmetric stretching vibration of phosphate (PO_4^{3-}) groups, which constitute the fundamental structural framework of hydroxyapatite. The result matches a previous report from Van-Pham *et al.*, who reported characteristic P-O absorption bands of PO_4^{3-} groups at 633 cm^{-1}, 1035 cm^{-1}, and 1995 cm^{-1} [43]. The band detected at 1668.12 cm^{-1} is associated with the bending vibration of adsorbed water molecules, indicating the presence of physically bound moisture on the sample surface. Meanwhile, the absorption at 1464.97 cm^{-1} and 1668.12 cm^{-1} confirms the presence of the carbonate (CO_3^{2-}) functional group.

The ZnO exhibited FTIR spectra at 3736.63 cm^{-1}, 3609.66 cm^{-1}, 2349.20 cm^{-1}, 1696.41 cm^{-1}, 1522.28 cm^{-1}, 872.20 cm^{-1}, 674.13 cm^{-1}, and 524.73 cm^{-1}. The strong absorption bands located at 674.13 cm^{-1} and 524.73 cm^{-1} are characteristic of Zn–O stretching vibrations in the ZnO lattice. The broad absorptions observed at 3736.63 cm^{-1} and 3609.66 cm^{-1} are attributed to the stretching vibrations of OH groups [44].

The FTIR analysis of ZnO/HA nanocomposite revealed that the IR spectra contained all of the distinctive bands of ZnO and HA. However, the new band at 522.70 cm^{-1} could be attributed to the adsorption peak of ZnO species in ZnO/HA [45]. An absorption band at approximately 2349 cm^{-1} was detected in all analyzed samples. This band is not associated with the intrinsic functional groups of the constituent materials but is more appropriately attributed to the asymmetric stretching vibration of atmospheric CO_2, which was likely adsorbed on the sample surface [46,47].

The crystalline structure and size of HA, ZnO, and ZnO/HA was examined via XRD, and their XRD patterns are presented in Figure 2. Figure 2 presents the XRD patterns of HA, ZnO, and the ZnO/HA composite. For HA, diffraction peaks were detected at 2θ values of 25.591°, 31.874°, 32.283°, 39.917°, 46.810°, and 49.557°. These reflections are consistent with the standard hydroxyapatite data (JCPDS No. 09-0432), which show characteristic peaks at 25.8° (002), 31.7°

(211), 32.9° (300), 46.7° (222), and 49.4° (213). The hexagonal phase of HA is typically identified by an intense peak near 31.7°, accompanied by adjacent reflections around 32.2° and 33.3°, confirming the formation of crystalline HA.

The XRD pattern of ZnO displays prominent peaks at 31.939°, 34.509°, 36.336°, 47.649°, 56.781°, 63.072°, 66.472°, 68.129°, 69.245°, 72.644°, 77.041°, 81.658°, and 89.792°. In accordance with JCPDS card No. 36-1451, the reflections at 31.939°, 34.509°, 36.336°, 47.649°, 56.781°, and 68.129° correspond to the (100), (002), (101), (110), (103), and (112) planes, respectively, indicating the typical wurtzite structure of ZnO. For the ZnO/HA composite, combined diffraction peaks were observed at 2θ values of 17.920°, 26.037°, 28.709°, 31.939°, 34.509°, 36.336°, 47.649°, 56.781°, 63.072°, 66.472°, 68.129°, 69.245°, 72.644°, 77.041°, 81.658°, and 89.792°, demonstrating the coexistence of both HA and ZnO crystalline phases in the composite material. The crystallite size of each sample was determined using the Scherrer equation [50].

$$D = \frac{K\lambda}{\beta cos\theta} \quad (2)$$

In this expression, D refers to the crystallite size (nm), K denotes the Scherrer constant with a typical value of 0.90, λ represents the wavelength of the Cu–Kα X-ray radiation (0.154 nm), β represents the full width at half maximum (FWHM) of the diffraction peak (in radians), and θ indicates the Bragg's angle associated with the diffraction peak. Based on X-ray diffraction data, the average crystallite size was calculated using the Scherrer equation, obtaining 25.66 nm for HA, 19.67 nm for ZnO, and 19.20 nm for ZnO/HA nanocomposites.

The surface characteristics and elemental composition of ZnO, HA, and the ZnO/HA nanocomposite were examined using SEM–EDX analysis. Figure 3 presents the morphological features of pure ZnO, pure HA, and the distribution of ZnO particles on the HA surface. SEM analysis reveals that ZnO exhibits a rod-shaped morphology characterized by a porous and moderately rough surface, implying the presence of hollow features and partial aggregation of particles. In contrast, hydroxyapatite (HA) prepared via the precipitation method predominantly shows a granular morphology with evident agglomeration. The compositional analysis obtained from EDX indicates an average Ca/P ratio of 1.67, which is in good agreement with the stoichiometric value of hydroxyapatite. In the ZnO/HA nanocomposite, SEM images display agglomerated granular nanoparticles with a rough and porous texture. The ZnO phase is well distributed throughout the hydroxyapatite matrix, forming a heterogeneous architecture that is expected to improve adsorption capability and photocatalytic activity by enlarging the effective surface area and strengthening interfacial interactions. Elemental mapping further confirms the spatial distribution of each component, where Zn species derived from ZnO are represented in yellow regions and Ca originating from HA appears in cyan regions, verifying the successful incorporation of ZnO onto the HA support.

The EDX spectra for the ZnO/HA nanocomposite, as presented in Figure 4, confirm the presence of all the expected elements (Zn, Ca, P, and O) specific to the HA and ZnO components. The detection of carbon (C) is likely attributed to the adsorption of atmospheric carbon dioxide (CO_2) on the surface of hydroxyapatite.

3.2 Photocatalytic Degradation Studies of RRRB Dye

The fundamental mechanism of photocatalytic degradation of azo dyes begins when ZnO is irradiated with light of sufficient energy, generating electrons in the conduction

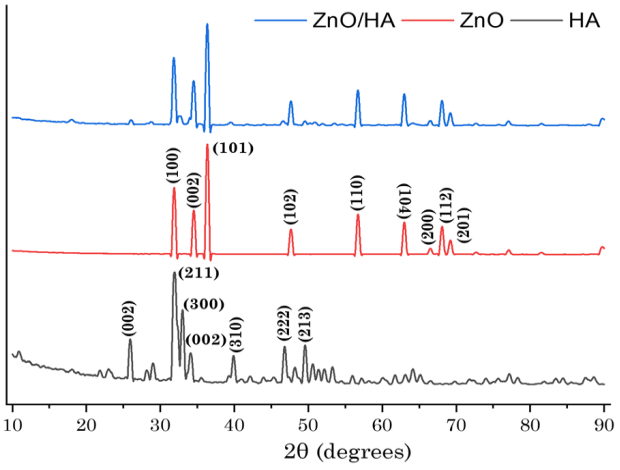

Figure 2. The XRD diffraction profiles for HA, ZnO and the ZnO/HA nanocomposite.

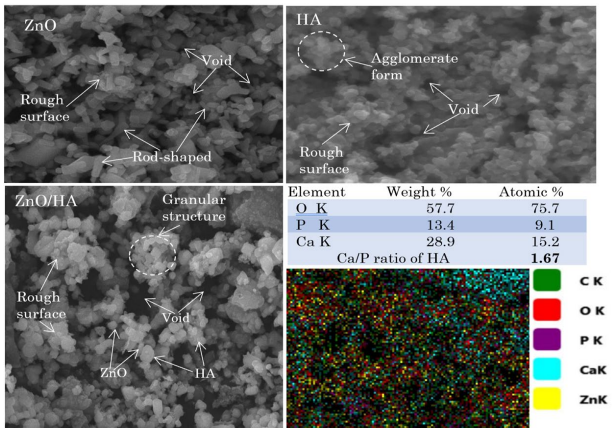

Figure 3. SEM-EDX images of ZnO, HA and ZnO/HA nanocomposite.

band (e^-) and holes in the valence band (h^+). The photogenerated holes (h^+) oxidize surface-adsorbed H_2O or OH^- to produce hydroxyl radicals ($\cdot OH$), while the conduction band electrons (e^-) reduce molecular oxygen (O_2) to form superoxide radicals ($\cdot O_2^-$). In the presence of protons (H^+), superoxide radicals can subsequently generate hydroperoxyl radicals ($HO_2\cdot$) and hydrogen peroxide (H_2O_2). Furthermore, the reaction between $\cdot O_2^-$ and H_2O_2 leads to the formation of additional hydroxyl radicals [51,52].

$$ZnO + h\nu \rightarrow e^-_{CB} + h^+_{VB} \quad (3)$$
$$h^+_{VB} + H_2O \rightarrow \cdot OH + H^+ \quad (4)$$
$$h^+_{VB} + OH^- \rightarrow \cdot OH \quad (5)$$
$$e^-_{CB} + O_2 \rightarrow \cdot O_2^- \quad (6)$$
$$\cdot O_2^- + H^+ \rightarrow HO_2\cdot \quad (7)$$
$$HO_2\cdot + HO_2\cdot \rightarrow H_2O_2 + O_2 \quad (8)$$
$$H_2O_2 + \cdot O_2^- \rightarrow \cdot OH + OH^- + O_2 \quad (9)$$

Hydroxyl radicals are the primary reactive species responsible for the breakdown of azo dye molecules. The RRRB, classified as an azo dye, contains the characteristic functional group represented by the general structure R_1-N=N-R_2. These reactive species attack and cleave the azo linkage, transforming the original azo dye into simpler end products, H_2O and CO_2 [53].

$$\cdot OH + R_1\text{-}N{=}N\text{-}R_2 \rightarrow R_1\text{-}NH_2 + R_2\text{-}NH_2 \text{ (aromatic amines)} \quad (10)$$
$$\cdot OH + \text{aromatic amines} \rightarrow \text{Simple degradation product} + CO_2 + H_2O \quad (11)$$

In this study, 300 mL of RRRB solution at a concentration of 25 mg/L was treated separately with 2 g of pristine ZnO and 2 g of the ZnO/HA nanocomposite at an initial pH of 7 and irradiated with both UV and visible light for 120 minutes. The purpose of this investigation was to evaluate the role of HA as a support material in enhancing the photocatalytic performance of ZnO for dye degradation. The resulting photodegradation efficiencies are presented in Figure 5.

The results in Figure 5 show that the ZnO/HA nanocomposite exhibited superior photocatalytic activity compared with pristine ZnO under both UV and visible light exposure. Under UV irradiation, the removal efficiency of RRRB reached 90.78% in the presence of ZnO/HA, slightly higher than that achieved by ZnO alone (89.15%). A more pronounced difference was observed under visible light, where the nanocomposite achieved 80.75% degradation, whereas pure ZnO showed only 10.53% removal efficiency. Integrating ZnO with hydroxyapatite markedly enhances its photocatalytic efficiency for dye degradation under light irradiation. Owing to its large specific surface area, hydroxyapatite provides abundant adsorption sites that facilitate close contact between dye molecules and the active ZnO surface. Moreover, hydroxyapatite exhibits a point of zero charge (pH_{pzc}) of approximately 8.61 [54], therefore, at pH values below this point, its surface becomes positively charged. This positive surface charge promotes strong electrostatic attraction toward RBBB, an anionic azo dye, thereby improving pollutant adsorption and accelerating the degradation process. In addition, the heterojunction formed between ZnO and hydroxyapatite enhances the separation of photogenerated electron–hole pairs, suppresses their recombination, and sustains higher photocatalytic activity compared with pristine ZnO [55,56]. This finding is consistent with Vaizogullar's results, who reported that ZnO/Bent has superior photocatalytic degradation compared to ZnO in degrading the oxytetracycline antibiotic under UV light [57]. In addition, research by Zhang *et al.* demonstrated that TiO_2/MXene composites enhance both the degradation efficiency and the degradation rate of methylene blue dye [58].

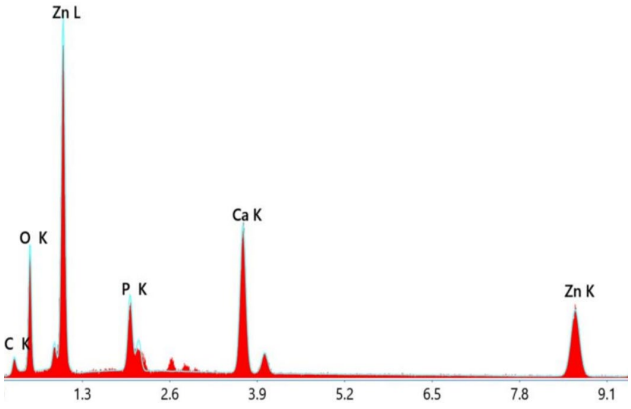

Figure 4. EDX spectra for ZnO/HA nanocomposite powder.

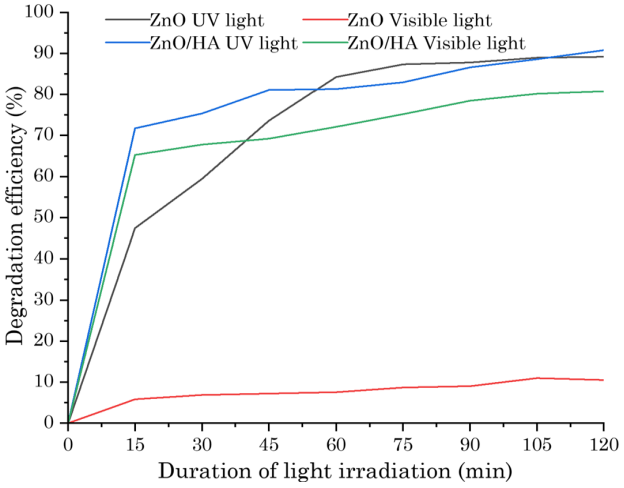

Figure 5. Degradation efficiency of dye with ZnO and ZnO/HA.

3.3. Effect of ZnO/HA Dose on Photocatalytic Degradation Efficiency

To evaluate the influence of catalyst loading on photocatalytic performance, 300 mL of RRRB solution (25 mg/L) was placed in the photoreactor. The solution pH was adjusted to 7 prior to adding varying amounts of ZnO/HA nanocomposite (1.0, 1.5, 2.0, and 2.5 g). The corresponding degradation efficiencies of RRRB at different catalyst dosages are presented in Figure 6. Catalyst loading plays a vital role in determining photocatalytic performance. Increasing the amount of photocatalyst generally provides more active sites in the reaction system, thereby promoting greater photon absorption and enhancing the formation of reactive species such as hydroxyl and superoxide radicals. Nevertheless, excessive catalyst addition may adversely affect performance. Higher solid concentrations can increase solution turbidity, intensify light scattering, and ultimately limit photon penetration to the catalyst surface [59]. As illustrated in Figure 6, raising the ZnO/HA dosage from 1.0 g to 2.0 g significantly improved the photocatalytic activity, which can be attributed to the greater availability of active sites. However, when the dosage was further increased to 2.5 g, only a slight enhancement in degradation efficiency was observed, likely due to restricted light transmission within the suspension. This finding is in accordance with the research of Bekhit *et al.* who reported that there was an increase in the efficiency of tetracycline photocatalytic degradation along with increasing MgONPs dosage from 0.1 to 0.6 g/L and then tended to decrease with the addition of 1.0 g/L [60].

3.4. Impact of pH on photocatalytic degradation performance

The solution's pH is a key factor in photocatalytic processes because it controls the surface charge of the semiconductor photocatalyst. At this stage, a 300 mL RRRB dye solution of 25 mg/L concentration was converted with a ZnO/HA photocatalyst mass of 2 g. The degradation efficiency of the dye at different pH conditions (4-10) is presented in Figure 7.

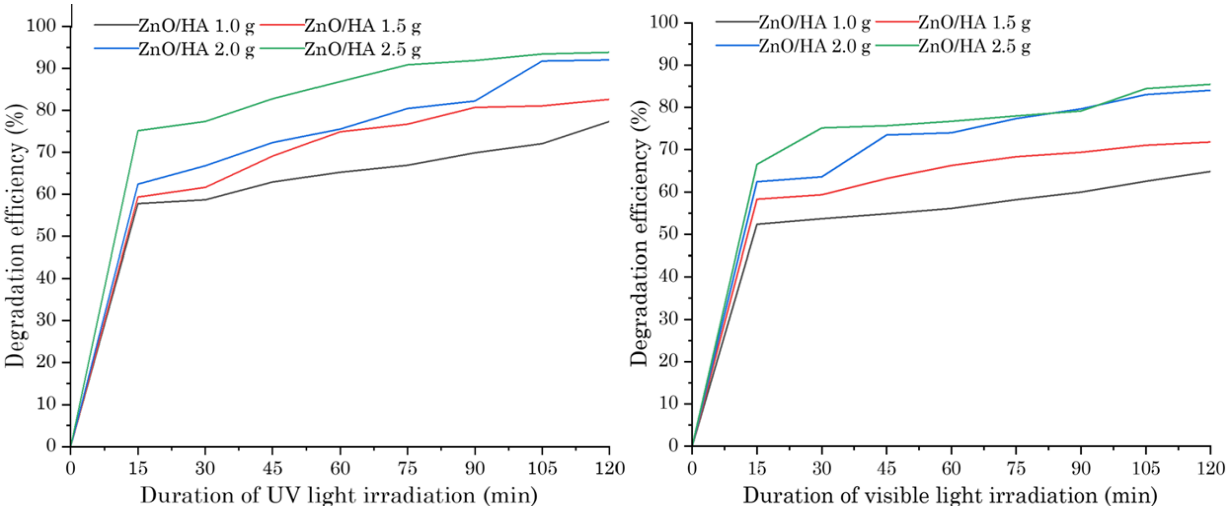

Figure 6. Effect of ZnO/HA dose on photocatalytic degradation efficiency.

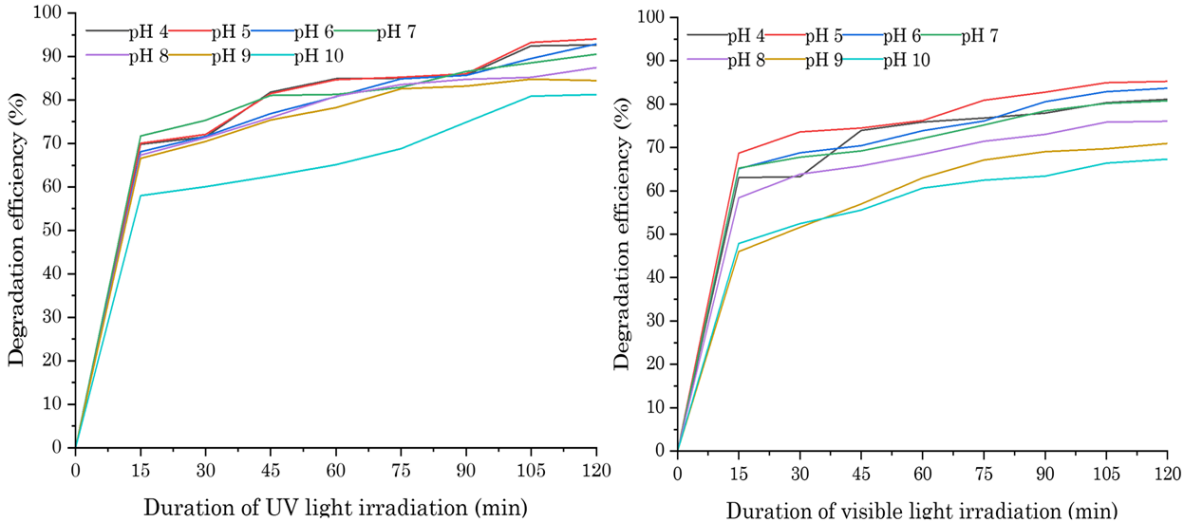

Figure 7. Photocatalytic degradation efficiency at different pH.

The degradation efficiency of RRRB initially increased and then declined as the pH was raised from 5 to 10, with the highest removal achieved at pH of 5. The degradation efficiency of RRRB initially increased and then declined as the pH was raised from 5 to 10, with the highest removal achieved at pH of 5. The influence of pH on the photocatalytic performance of the ZnO/HA composite can be explained by considering the point of zero charge (pH_{PZC}) and the resulting surface charge of the catalyst. According to Alhasan *et al.*, ZnO has a pH_{PZC} of 8.4, indicating that its surface is positively charged at pH values below 8.4 due to protonation and negatively charged at pH values above 8.4 [61]. Under acidic conditions, the abundance of H^+ ions promotes protonation of the ZnO/HA surface, making it more positively charged. This enhances electrostatic attraction between the positively charged catalyst surface and the anionic RRRB dye molecules, facilitating stronger adsorption and improved photocatalytic degradation. In contrast, at alkaline pH, both the ZnO/HA surface and the anionic dye carry negative charges, resulting in electrostatic repulsion. This repulsive interaction reduces dye adsorption onto the catalyst surface and consequently lowers the degradation efficiency [62].

3.5. Impact of Initial Dye Concentration on Photocatalytic Degradation Performance

Studying the effect of dye concentration on photocatalytic performance is very important for the practical design of photocatalytic treatment units. At this point, 300 mL of RRRB dye solution with concentrations ranging from 25 to 75 mg/L was subjected to treatment with 2 grams of a ZnO/HA nanocomposite. The photocatalytic reaction process was performed at pH of 5 using separate 50-watt UV and visible light irradiation for 120 min, with dye color removal monitored every 15 min of treatment.

The efficiency of dye degradation is presented in Figure 8. Figure 8 illustrates that higher dye concentrations resulted in lower photocatalytic degradation efficiency. When the dye concentration was raised from 25 mg/L to 75 mg/L, the removal efficiency dropped from 94.06% to 70.90% under UV light and from 81.37% to 61.83% under visible light, with a consistent treatment time of 120 min. This study found that the optimal concentration of dye that can be processed to produce optimum efficiency is 50 mg/L at an initial pH treatment condition of 5, with 2 g of ZnO/HA nanocomposite. Under these conditions, the degradation efficiency for the reactor irradiated with UV and visible light for 120 min was 90.43% and 80.93%, respectively. At higher dye concentrations, photocatalytic degradation efficiency often declines because the dye molecules can absorb most of the light, hindering it from reaching the photocatalyst [63]. This reduced light absorption limits the formation of electron-hole pairs, which are essential for the degradation process [64]. Previous work conducted by Sukarta *et al.* also demonstrated that the photocatalytic degradation efficiency of rhodamine B using HA–ZnO composite under UV irradiation declined noticeably as the initial dye concentration increased [65].

4. Conclusions

In this study, a photocatalytic reaction using a 1:1 ZnO/HA nanocomposite effectively degraded 300 mL of 50 mg/L Remazol RRB solution. Irradiation with 50 watts of UV and visible light for 120 minutes at pH of 5 resulted in degradation efficiencies of 90.43% and 80.93%, respectively. Thus, ZnO/HA composite can be effectively utilized as a cheaper natural supporting catalyst for the removal of dye from aqueous medium.

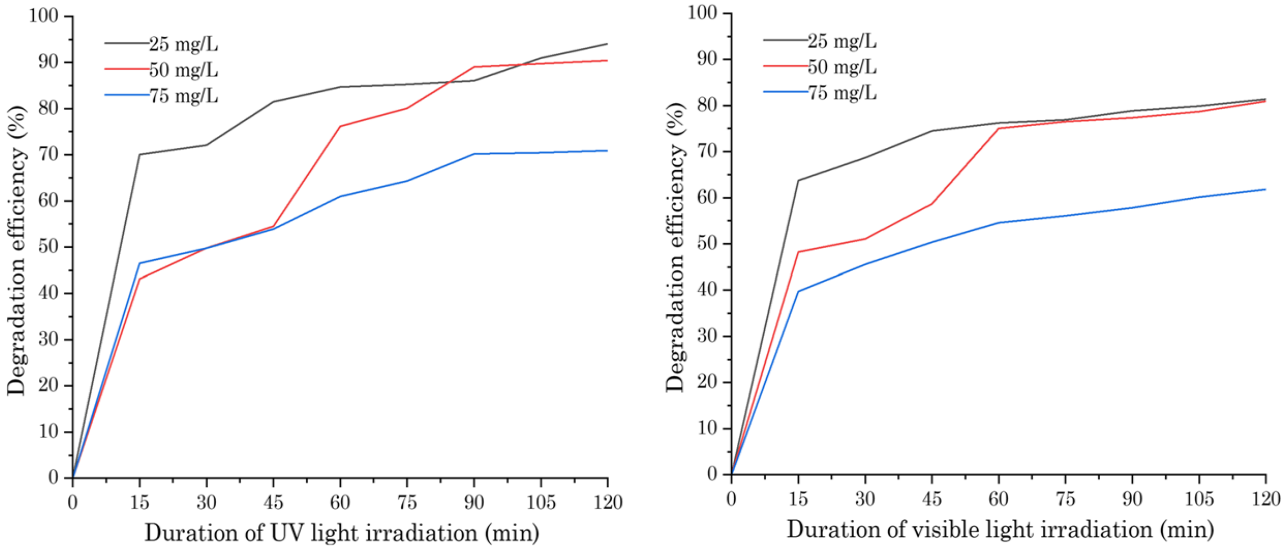

Figure 8. Effect of dye concentration on photocatalytic degradation efficiency.

Acknowledgment

This research was financially supported by the Research and Community Service Universitas Pendidikan Ganesha, with contract number 1254/UN48.16/LT/2024. All the authors thank the Chemistry Department for laboratory facilities.

CRedit Author Statement

Author Contributions: I Dewa Ketut Sastrawidana: Conceptualization, Design of methodology, Resources, Investigation, Writing-initial draft preparation; Luh Putu Ananda Saraswati: Resources, Investigation, Data curation, Formal analysis; I Nyoman Sukarta: Formal analysis, Investigation, Data presentation, Review and editing manuscript; Ni Made Wiratini: Software, Formal analysis, Review and editing of manuscript; I Ketut Sudiana: Formal analysis, Review and editing of manuscript; I Wayan Suja: Resources, Data curation, Review and editing of manuscript. All authors have read and agreed to the published version of the manuscript.

References

[1] Panhwar, A., Jatoi, A.S., Mazari, S.A., Kandhro, A., Rashid, U., Qaisar, S. (2024). Water resources contamination and health hazards by textile industry effluent and glance at treatment techniques: A review. *Waste Management Bulletin*. 1 (4), 15-163. DOI: 10.1016/j.wmb.2023.09.002.

[2] Majeed, F., Razzaq, A., Rehmat, S., Azhar, I., Mohyuddin, A., Rizvi, N.B. (2024). Enhanced dye sequestration with natural polysaccharides-based hydrogels: A review. *Carbohydrate Polymers*. 330, 121820. DOI: 10.1016/j.carbpol.2024.121820.

[3] Lawal, I.M., Soja, U.B., Hussaini, A., Saleh, D., Aliyu, M., Noor, A, Birniwa, A.H., Jagaba, A.H. (2023). Sequential batch reactors for aerobic and anaerobic dye removal: A mini-review. *Case Studies in Chemical and Environmental Engineering*. 8, 100547. DOI: 10.1016/j.cscee.2023.100547.

[4] Periyasamy, A.P (2024). Recent advances in the remediation of textile-dye-containing wastewater: Prioritizing human health and sustainable wastewater treatment. *Sustainability*. 16 (495), 2-41. DOI: 10.3390/su16020495.

[5] Sastrawidana, I.D.K., Rachmawati, D.O., Sudiana, I.K. (2018). Color removal of textile wastewater using indirect electrochemical oxidation with multi carbon electrodes. *EnvironmentAsia*. 11 (3), 170-181. DOI: 10.14456/ea.2018.46.

[6] Marszałek, J., Zyłła, R. (2021). Recovery of water from textile dyeing using membrane filtration. *Processes*. 9, 1833. DOI: 10.3390/pr9101833.

[7] Sudiana, I.K., Sastrawidana, I.D.K., Sukarta, I.N. (2022). Adsorption kinetic and isotherm studies of reactive red B textile dye removal using activated coconut leaf stalk. *Ecological Engineering & Environmental Technology*. 23 (5), 61-71. DOI: 10.12912/27197050/151628.

[8] Pradeebaa, S.J., Sampath, K. (2022). Photodegradation, thermodynamic and kinetic study of cationic and anionic dyes from effluents using polyazomethine/ZnO and polyazomethine/TiO2 nanocomposites. *Journal of Optoelectronic and Biomedical Materials*. 14 (3), 89–105. DOI: 10.15251/JOBM.2022.143.89.

[9] Nidheesh, P.V., Divyapriya, G., Titchou, F.E., Hamdani, M. (2022). Treatment of textile wastewater by sulfate radical based advanced oxidation processes. *Separation and Purification Technology*. 293, 121115. DOI: 10.1016/j.seppur.2022.121115.

[10] Tianzhi, W., Weijie, W., Hongying, H., Khu, S.T. (2023). Effect of coagulation on bio-treatment of textile wastewater: Quantitative evaluation and application. *Journal of Cleaner Production*. 312, 127798. DOI: 10.1016/j.jclepro.2021.127798.

[11] Sukarta, I.N., Ayuni, N.P.S., Sastrawidana, I.D.K. (2021). Utilization of Khamir (Saccharomyces cerevisiae) as adsorbent of remazol red RB textile dyes. *Ecological Engineering & Environmental Technology*. 22 (1), 117-123. DOI: 10.12912/27197050/132087.

[12] Sudiana, I.K., Citrawathi, D.M., Sastrawidana, I.D.K., Maryam, S., Sukarta, I.N., Wirawan, G.A.H. (2022). Biodegradation of turquoise blue textile dye by wood degrading local fungi isolated from plantation area. *Journal of Ecological Engineering*. 23(7), 205–214. DOI: 10.12911/22998993/150044.

[13] Rawat, D., Sharma, U., Yadav, A., Poria, P., Farooqi, F., Pani, B., Mukherjee, P., Singh, M., Sharma, R.S., Mishra, V. (2023). A bottom-up approach to select microbes from textile wastewater for detoxification of aromatic amine and azo dye in a single stage. *Journal of Water Process Engineering*. 53, 103668. DOI: 10.1016/j.jwpe.2023.103668.

[14] Zeid, S.A., Leprince-Wang, Y. (2024). Advancements in ZnO-based photocatalysts for water treatment: A comprehensive review. *Crystals*. 14, 611. DOI: 10.3390/cryst14070611.

[15] Sagadevan, S., Fatimah, I., Egbosiub, T.C., Alshahateet, S.F., Lett, J.A., Weldegebrieal, G.K., Le, M.V., Johan, M.R. (2022). Photocatalytic efficiency of titanium dioxide for dyes and heavy metals removal from wastewater. *Bulletin of Chemical Reaction Engineering & Catalysis*. 17(2), 430-450. DOI: 10.9767/bcrec.17.2.13948.430-450.

[16] Chairungsri, W., Subkomkaew, A., Kijjanapanich, P., Chimupala, Y. (2022). Direct dye wastewater photocatalysis using immobilized titanium dioxide on fixed substrate. *Chemosphere*. 286 (2), 131762. DOI: 10.1016/j.chemosphere.2021.131762.

[17] Shareef, S., Mushtaq, A. (2023). Wastewater treatment by photocatalysis: Approaches, mechanisms, applications, and challenges. *International Journal of Chemical and Biochemical Sciences*. 24 (4), 278-286.

[18] Zhang, S., Cai, M., Wu, J., Wang, Z., Lu, X., Li, K., Lee, J.M., Min, Y. (2023). Photocatalytic degradation of TiO2 via incorporating Ti3C2 MXene for methylene blue removal from water. *Catalysis Communications*. 174, 106594. DOI: 10.1016/j.catcom.2022.106594.

[19] Navidpour, A.H., Fakhrzad, M., Tahari, M., Abbasi, S. (2018). Novel photocatalytic coatings based on tin oxide semiconductor. *Surface Engineering*. 35 (3), 216-226. DOI: 10.1080/02670844.2018.1477559.

[20] Ramanathan, G., Murali, K.R. (2022). Photocatalytic activity of SnO2 nanoparticles. *Journal of Applied Electrochemistry*. 52, 849–859. DOI: 10.1007/s10800-022-01676-z.

[21] Khadka, D., Gautam, P., Dahal, R., Ashie, M.D., Paudyal, H., Ghimire, K.N., Pant, B., Poudel, B.R., Bastakoti, B.P., Pokhrel, M.R. (2024). Evaluating the photocatalytic activity of green synthesized iron oxide nanoparticles. *Catalysts*. 14, 751. DOI: 10.3390/catal14110751

[22] Solymos, K., Babcsanyi, I., Ariya, B., Gyulavari, T., Ágoston, A., Szamosvolgyi, A., Kukovecz, A., Konya, Z., Farsang, A., Pap, Z. (2024). Photocatalytic and surface properties of titanium dioxide nanoparticles in soil solutions. *Environmental Science: Nano*. 11, 1204. DOI: 10.1039/d3en00622k.

[23] Dihom, H.R., Al-Shaibani, M.M., Mohamed, R.M.S.R., Al-Gheethi, A.A., Sharma, A., Khamidun, M.H.B. (2022). Photocatalytic degradation of disperse azo dyes in textile wastewater using green zinc oxide nanoparticles synthesized in plant extract: A critical review. *Journal of Water Process Engineering*. 47, 102705. DOI: 10.1016/j.jwpe.2022.102705.

[24] Santana-Camacho, D., Barrios-Navarro, F.A., Moreno-Meza, A., Villegas-Fuentes, A., Vilchis-Nestor, A.R., Luque, P.A. (2024). Photocatalytic properties of ZnO semiconductor nanoparticles green synthesized employing Ipomoea stans leave extracts. *Ceramics International*. 50 (21), 44426-44439. DOI: 10.1016/j.ceramint.2024.08.290.

[25] Hosseini, M., Ghanbari, M., Dawi, E.A., Altimari, U.S., Aljeboree, A.M., Salavati-Niasari, M. (2024). Synthesis and characterization of zinc stannate decorated on graphitic carbon nitride and study its potential for degradation of Eriochrome Black T and erythrosine under simulated sunlight. *Arabian Journal of Chemistry*. 17 (1), 105395. DOI: 10.1016/j.arabjc.2023.105395.

[26] Wang, K., Guan, Z., He, Y., Fa,n M. (2025). Harnessing zinc stannate for sustainable energy and environment solutions: Advances in photocatalytic, piezocatalytic, and piezo-photocatalytic technologies. *Nano Energy*. 133, 110518. DOI: 10.1016/j.nanoen.2024.110518.

[27] Rajaraman, T.S., Parikh, S.P., Gandhi, V.G. (2020). Black TiO2: A review of its properties and conflicting trends. *Chemical Engineering Journal*. 389, 123918. DOI: 10.1016/j.cej.2019.123918.

[28] Zhou, S., Jiang, L., Wang, H., Yang, J., Yuan, X., Wang, H., Liang, J., Li, X., Li, H., Bu, Y. (2023). Oxygen vacancies modified TiO2/O-terminated Ti3C2 composites: Unravelling the dual effects between oxygen vacancy and high-work-function titanium carbide. *Advanced Functional Materials*. 33 (41), 2307702. DOI: 10.1002/adfm.202307702.

[29] Zeid, S.A., Perez, A., Bastide, S., Le Pivert, M., Rossano, S. (2024). Antibacterial and photocatalytic properties of ZnO nanostructure decorated coatings. *Coatings*. 14 (1), 41. DOI: 10.3390/coatings14010041.

[30] Pekarek, S., Mikes, J., Krysa, J. (2015). Comparative study of TiO2 and ZnO photocatalysts for the enhancement of ozone generation by surface dielectric barrier discharge in air. *Applied Catalysis A: General*. 502, 122-128. DOI: 10.1016/j.apcata.2015.06.003.

[31] Turkten, N., Bekbolet, M. (2020). Photocatalytic performance of titanium dioxide and zinc oxide binary system on degradation of humic matter. *Journal of Photochemistry and Photobiology A: Chemistry*. 401, 112748. DOI: 10.1016/j.jphotochem.2020.112748.

[32] Baig, A., Siddique, M., Panchal, S. (2025). A review of visible-light-active zinc oxide photocatalysts for environmental application. *Catalysts*. 15 (2), 100. DOI: 10.3390/catal15020100.

[33] Le, A.T., Le, T.D.H., Cheong, K.Y., Pung, S.Y. (2022). Immobilization of zinc oxide-based photocatalysts for organic pollutant degradation: A review. *Journal of Environmental Chemical Engineering*. 10 (5), 108505. DOI: 10.1016/j.jece.2022.108505.

[34] Humayoun, U.B., Mehmood, F., Hassan, Y., Rasheed, A., Dastgeer, G., Anwar, A., Sarwar, N., Yoon, D. (2023). Harnessing bio-immobilized ZnO/CNT/chitosan ternary composite fabric for enhanced photodegradation of a commercial reactive dye. *Molecules*. 28 (18), 6461. DOI: 10.3390/molecules28186461.

[35] Asiri, A.M., Pugliese, V., Coppola, G., Khan, S.B., Alamry, K.A., Alfifi, S.Y., Marwani, A.M., Alotaibi, M.M., Petrosino, F., Chakraborty, S. (2024). Zinc oxide nanoparticles immobilized on polymeric porous matrix for water remediation. *Emergent Materials*. 7, 1531–1544. DOI: 10.1007/s42247-024-00728-8.

[36] Khataee, A., Kiransan, M., Karaca, S., Arefi-Oskoui, A. (2016). Preparation and characterization of ZnO/MMT nanocomposite for photocatalytic ozonation of a disperse dye. *Turkish Journal of Chemistry*. 40, 546-564. DOI: 10.3906/kim-1507-77.

[37] Shaik, B.B., Katari, N.K., Raghupathi, J.K., Jonnalagadda, S.B., Rana, S. (2024). Titanium dioxide/graphene-based nanocomposites as photocatalyst for environmental applications: A review. *ChemistrySelect*. 9, e202403521. DOI: 10.1002/slct.202403521.

[38] Wang, Z.D., Xia, T., Hua-Li, Z., Shao, M.F. (2024). A review of carbon-based catalysts and catalyst supports for simultaneous organic electro-oxidation and hydrogen evolution reactions. *New Carbon Materials*. 39 (1), 67-77. DOI: 10.1016/S1872-5805(24)60829-2.

[39] Dhayal, M., Sharma, S., Jakhar, P., Sain, Y., Sharma, H. (2025). Carbon-supported photocatalysts: A sustainable approach for enhanced environmental remediation. *Comments on Inorganic Chemistry*. 1–55. DOI: 10.1080/02603594.2025.2494273

[40] Rajesh, M., Minh, D.P., Ange, N. (2020). Hydroxyapatite as a new support material for cobalt-based catalysts in Fischer-Tropsch synthesis. *International Journal of Hydrogen Energy*. 45 (36), 18440-18451. DOI: 10.1016/j.ijhydene.2019.09.043.

[41] Zheng, M., Zhou, F., Ma, H., Song, X., Wu, G. (2024). Hydroxyapatite supported molybdenum oxide catalyst for selective dehydrogenation of cyclohexane to cyclohexene: studies of dispersibility and chemical environment. *Royal Society of Chemistry*. 14, 36461–36470. DOI: 10.1039/D4RA06259K.

[42] Sukarta, I.N., Sastrawidana, I.D.K. (2024). Synthesis and characterization of hydroxyapatite/titania composite and its application on photocatalytic degradation of remazol red B textile dye under UV irradiation. *Ecological Engineering & Environmental Technology*. 25 (2), 178-189. DOI: 10.12912/27197050/176230.

[43] Van-Pham, D.T., Phat, V.V., Chiem, N.H., Quyen, T.T.B., Mai, N.T.N., Giao, D.H., Don, T.N., Thien, D.V.H. (2022). Synthesis of hydroxyapatite/Zinc Oxide nanoparticles from fish scales for the removal of hydrogen sulfide. *Environment and Natural Resources Journal*. 20 (3), 323-329. DOI: 10.32526/ennrj/20/202100228.

[44] Bashir, S., Awan, M.S., Farrukh, M.A., Naidu, R., Khan, S.A., Rafique, N., Ali, S., Hayat, I., Hussain, I., Khan, M.Z. (2022). In-vivo (Albino mice) and in-vitro assimilation and toxicity of zinc oxide nanoparticles in food materials. *International Journal of Nanomedicine*. 17, 4073–4085. DOI: 10.2147/IJN.S372343.

[45] Buazar, F., Alipouryan, S., Kroushawi, F., Hossieni, S.A. (2015). Photodegradation of odorous 2-mercaptobenzoxazole through zinc oxide/hydroxyapatite nanocomposite. *Applied Nanoscience*. 5, 719–729. DOI: 10.1007/s13204-014-0368-4.

[46] Fattah, Z.A. (2016). Synthesis and characterization of Nickel doped Zinc Oxide nanoparticles by sol-gel method. International *Journal of Engineering Sciences and Research Technology*. 5(7), 418-429. DOI: 10.5281/zenodo.56998.

[47] Abifarin, J.K., Obada, D.O., Dauda, E.T., Dodoo-Arhin, D. (2019). Experimental data on the characterization of hydroxyapatite synthesized from biowastes. *Data in Brief*. 26, 104485. DOI: 10.1016/j.dib.2019.104485.

[48] Florkiewicz, W., Słota, D., Placek, A., Pluta, K., Tyliszczak, B., Douglas, T.E.L., Sobczak-Kupiec, A. (2021). Synthesis and characterization of polymer-based coatings modified with bioactive ceramic and bovine serum albumin. *Journal of Functional Biomaterials*. 12(2), 21. DOI: 10.3390/jfb12020021.

[49] Kumar, K.C.V., Subha, T.J., Ahila, K.G., Ravindran, B., Chang, S.W., Mahmoud, A.H., Mohammed, O.B., Rathi, M.A. (2021). Spectral characterization of hydroxyapatite extracted from black Sumatra and fighting cock bone samples: A comparative analysis. *Saudi Journal of Biological Sciences*. 28, 840-846. DOI: 10.1016/j.sjbs.2020.11.020.

[50] Azad, Md.A.S., Hossain, Md.S., Saikat, S.P., Hasan, Md.R., Bhowmik, S. (2025). Structural insights into zinc oxide–silver nanocomposite via different XRD models: rapid synthesis with photocatalytic & antibacterial applications. *Nanoscale Advances*. 7, 8138. DOI: 10.1039/d5na00790arsc.li/nanoscale-advances.

[51] Sun, Y., Zhang, W., Li, Q., Liu, H., Wang, X. (2023). Preparations and applications of zinc oxide based photocatalytic materials. *Advanced Sensor and Energy Materials*. 2 (3), 100069. DOI: 10.1016/j.asems.2023.100069.

[52] Nedelkovski, V., Radovanovic, M., Antonijevic, M. (2025). Advances in photocatalytic degradation of crystal violet using ZnO-based nanomaterials and optimization possibilities: A review. *ChemEngineering*. 9, 120. DOI: 10.3390/chemengineering9060120.

[53] Kumar, J.E., Sahoo, M.K. (2024). A review on effect of operational parameters for the degradation of azo dyes by some advanced oxidation processes. *Sustainable Chemistry for the Environment*. 11, 100274. DOI: 10.1016/j.scenv.2025.100274.

[54] Sagar, B.M., Parhad, T.H., Habib, Md.L., Ahmed, S., Hossain, Md.S. (2025). Synthesis of complex metal-doped nano-hydroxyapatite (HAp) for adsorptive removal of textile effluents. *Next Nanotechnology*. 8, 100310. DOI: 10.1016/j.nxnano.2025.100310.

[55] Sowndharya, S., Nikitha, M., Meenakshi, S.S. (2025). Designing an in-situ embedment of citric acid@HAp/ZnO as a Z-scheme heterojunction for substantial enhancement in photocatalytic degradation of malachite green under visible light. *Journal of Cleaner Production*. 490, 144723. DOI: 10.1016/j.jclepro.2025.144723.

[56] Manikandan, K., Kumar, N.D., Velmurugan, R., Gokulnath, M., Parvathy, S., Ayyar, M., Swaminathan, M., Prabhu, P., Alhuthali, A.M.S., Abdellattif, M.H., Haldhar, R., Hossain, M.K. (2025). Enhanced efficiency of zinc oxide hydroxyapatite nanocomposite in photodegradation of methylene blue, ciprofloxacin, and in wastewater treatment. *Scientific Reports*. 15, 31819. DOI: 10.1038/s41598-025-14310-7

[57] Vaizogullar, A.I. (2018). Comparing photocatalytic activity of ZnO and nanospherical ZnO/bentonite catalyst: Preparation, structural characterization and their photocatalytic performances using oxytetracycline antibiotic in aqueous solution. *Journal of the Mexican Chemical Society*. 62(1), 1-17. DOI: 10.29356/jmcs.v62i1.578.

[58] Zhang, S., Cai, M., Wu, J., Wang, Z., Lu, X., Li, K., Lee, J.M., Min, Y. (2023). Photocatalytic degradation of TiO2 via incorporating Ti3C2 MXene for methylene blue removal from water. *Catalysis Communications*. 174: 106594. DOI: 10.1016/j.catcom.2022.106594.

[59] Akinnawo, S.O., Ediagbonya, T.F. (2025). Advances on modification of photocatalyst for degradation/removal of organic pollutants from water. *Cleaner Chemical Engineering*. 11, 100176. DOI: 10.1016/j.clce.2025.100176.

[60] Bekhit, S.M., Zaki, S.A., Hassouna, M.S.D., Elkady, M. (2024). Combined effect of adsorption and photocatalytic degradation using Magnesium Oxide nano-flowers for tetracycline removal. *Journal of Inorganic and Organometallic Polymers and Materials*. 34, 5006–5019. DOI: 10.1007/s10904-024-03138-9.

[61] Alhasan, H.S., Omran, A.R., Al Mahmud, A., Mady, A.H., Thalji, M.R. (2024). Toxic congo red dye photodegradation employing green synthesis of Zinc Oxide nanoparticles using gum Arabic. *Water*. 16 (15), 2202. DOI: 10.3390/w16152202.

[62] Mei, J., Gao, X., Zou, J., Pang, F. (2023). Research on photocatalytic wastewater treatment reactors: Design, optimization, and evaluation criteria. *Catalysts*. 13 (6), 974. DOI: 10.3390/catal13060974.

[63] Ny Aina, A.R., Patel, H., Aich, S., Roy, B., Samanta, N.S., Pal, B. (2025). Recent advances in ZnO based photocatalysts for industrial dye degradation. *Discover Applied Sciences*. 7:977. DOI: 10.1007/s42452-025-07530-z.

[64] Poorsajadi, F., Sayadi, M.H., Hajiani, M., Rezaei, M.R. (2022). Synthesis of CuO/Bi2O3 nanocomposite for efficient and recycling photodegradation of methylene blue dye, International *Journal of Environmental Analytical Chemistry*. 102, 7165–7178. DOI: 10.1080/03067319.2020.1826464.

[65] Sukarta I.N., Suyasa, I.W.B., Mahardika, I.G., Suprihatin, I.E., Sastrawidana, I.D.K., Wiratma, I.G.L. (2025). Eco-friendly photocatalyst from limestone: ZnO-hydroxyapatite composite for efficient Rhodamine B removal. *Bulletin of Chemical Reaction Engineering & Catalysis*. 20 (3): 471-482. DOI: 10.9767/bcrec.20426.